UAS PHOTOGRAMMETRY AND OBJECT-BASED IMAGE ANALYSIS (GEOBIA): EROSION MONITORING AT THE KAZÁR BADLAND, HUNGARY

LÁSZLÓ BERTALAN* – ZOLTÁN TÚRI – GERGELY SZABÓ

University of Debrecen, Department of Physical Geography and Geoinformatics
H-4032 Debrecen, Egyetem tér 1. Hungary
*e-mail: bertalan@science.unideb.hu

Received 14 August 2016, accepted in revised form 12 September 2016

Abstract
A remarkable badland valley is situated near Kazár, NE-Hungary, where rhyolite tuff outcrops as greyish white cliffs and white barren patches. The landform is shaped by gully and rill erosion processes. We performed a preliminary state UAS survey and created a digital surface model and ortophotograph. The flight was operated with manual control in order to perform a more optimal coverage of the aerial images. The overhanging forests induced overexposed photographs due to the higher contrast with the bare tuff surface. The multiresolution segmentation method allowed us to classify the ortophotograph and separate the tuff surface and the vegetation. The applied methods and final datasets in combination with the subsequent surveys will be used for detecting the recent erosional processes of the Kazár badland.

Keywords: badland, photogrammetry, GEOBIA, UAS, erosion, gully, rill

1. Introduction

The geomorphological term 'badland' belongs to unique uncovered and shredded landscapes with steep slopes and high erosion rates being inappropriate for any kind of agricultural use (Nadal-Romero et al. 2007; Caraballo-Arias et al. 2015; Pintér et al. 2015). Geological and mainly the lithological factors have the main influence on the evolution of these landforms (Farabegoli – Agostini 2000; Neugirg et al. 2016) since the occurrence of badlands is significant on soft materials (Caraballo-Arias et al. 2015).

At the North-Eastern part of Hungary the badland forms are originated from the Gyulakeszi Rhyolite Tuff Formation as deposited materials of the Miocene volcanism (Pintér et al. 2015). However, the majority of the badlands are localized at humid areas (Caraballo-Arias et al. 2015) but the NE Hungarian badland areas are situated at the temperate or semi-humid climate zone without outstanding rainfall activity; thus, these landforms should have been formed at places where the vegetation cover had been violated due to anthropogenic processes i.e. deforestation and exhaustive grazing (Karátson 2006; Karancsi 2007; Horváth – Karancsi 2011).

The most extensive badland valley in Hungary is situated near the village of Kazár (Fig. 1). According to the ^{14}C age determination by Karátson (2006) this is a relatively young, 250 years old landform that had been emerged to the top by tectonic movements at Plio-Pleistocene. Pinter et al. (2015) described that the rhyolite tuffs outcrops here as greyish white cliffs and white barren patches (Fig. 2) and these surfaces

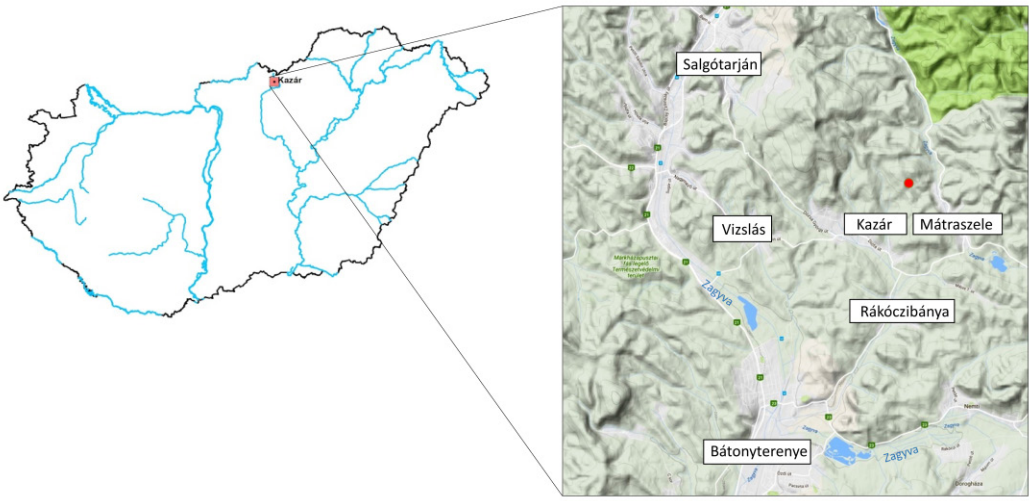

Fig. 1. The location of the Kazár badland valley

are strongly shaped by several erosional processes: weathering of non-welded tuff materials; hyper-concentrated mud-flows of wet argillized rock materials along the rills. Frost erosion is also a driving factor since the tuffs absorb considerably large amount of water; thus, physical weathering due to regelation and freeze-thaw frequently occurs (Regüés et al. 1995; Török et al. 2005).

Since this landform is sensitive for the environmental factors, then accelerated soil erosion (especially gullies and rills) processes affects their surface development (Conoscenti et al. 2008; Nadal-Romero et al. 2014; Caraballo-Arias et al. 2015). The NE Hungarian badlands are unique landforms in the Carpathian Basin; therefore, it is quite topical to reveal the recent degradation processes there. High resolution digital elevation models are the essential elements for the majority of the calculations and models referring to watershed analysis (Czigány et al. 2013), valley development (Telbisz et al. 2012), soil erosion and badland morphology (Conoscenti et al. 2008, 2014; Lopez Saez et al. 2011) that could be combined with several other factors as well (i.e. lithology, land use) for delineating the erosion susceptible areas for instance.

Although remote sensing applications are widely used for detailed monitoring of several erosion processes, the related capital and logistical costs could be relatively high (Westoby et al. 2012). But UAS-based small format aerial photography and the Structure-from-Motion (SfM) photogrammetry provides fast and cheap methods for surface reconstruction (Aber et al. 2010; Westoby et al. 2012; Nadal-Romero et al. 2015). In the case of small scale badland areas, like the Kazár badlands in Hungary, the use of Unmanned Aerial Systems (UAS) proved that these systems can provide more practical area-specific ways of photogrammetric survey and cm-level resolution digital surface or elevation models (d'Oleire-Oltmanns et al. 2012; Colomina – Molina 2014; Gómez-Gutierrez et al. 2014; Stöcker et al. 2015; Mészáros et al. 2016). Object-based image analysis is an effective tool for the processing, interpretation and spatial analysis of these type of very high resolution (<1 m/pixel) remote sensing datasets (Dragut – Eisank 2012). It is more effective to create and classify image objects that represents partially or totally the elements of the real world than removing pixels from their environment and investigate them separately (Openshaw 1984; Blaschke – Strobl 2001; Czimber 2009).

The main objective of this study was threefold; (1) at first, to establish a

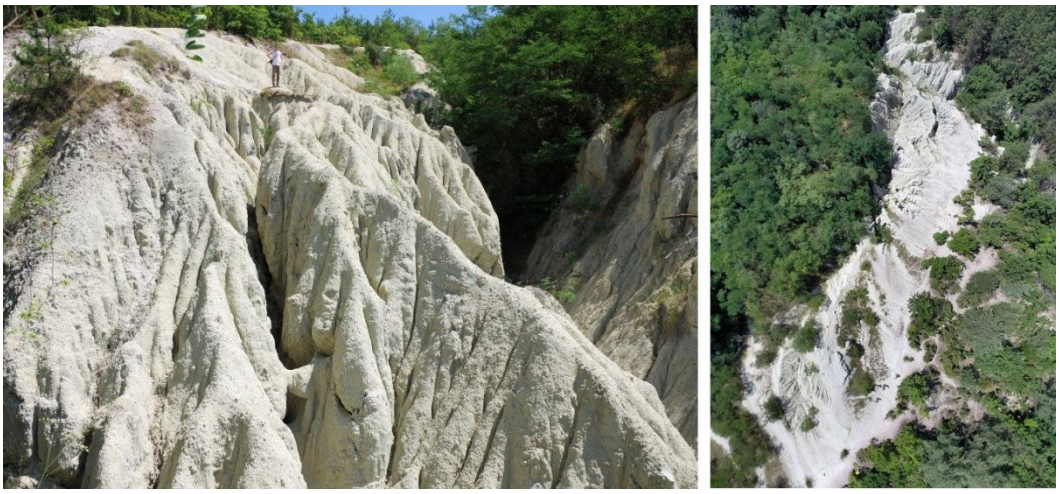

Fig. 2. Overview of the Kazár badland valley on terrestrial and aerial imagery

preliminary state UAS survey of the Kazár badlands that will be the base of further calculations on soil erosion processes that affects this landscape. (2) Moreover, our goal was to examine the specific conditions for the aerial imaging and GCPs at this type of high-contrast and high-relief tuff surface. (3) We also aimed to examine the potential applicability of geographic object-based image analysis (GEOBIA) on the generated ortophotographs for the analysis of erosion surfaces characterized by mosaicked land cover.

2. Materials and methods

The aerial survey for the photogrammetry-based surface reconstruction was performed at 30.07.2016 with a GoPro Hero 3 Black Edition camera mounted on a DJI Phantom-2 multicopter. The resolution of the pictures was 12 Mp with a field of view (FOV) 149° and a focal length of 2.77 mm. We captured 236 pictures from an average 33 m height during the 6 minutes long flight then we selected 194 pictures for the processing phase omitting the overexposed or blurry images. The UAS device was operated by a continuous ground control during the whole flight. Contrary to the automatic method, this method could provide more precise survey at an average landscape (Aber et al. 2010; Colomina – Molina 2014), the manual control of the UAS allowed to capture the images from the optimal height and angle above the previously described badland surface (Fig. 3). Accordingly, we applied this type of method, it became possible to capture the aerial photographs at two height levels considering the average slope gradient of the valley surface. Altogether, every part of the valley surface was covered by at least 10 pictures by aerial photographs from the UAS flight.

Despite the advantages of the above mentioned method, not enough amount of pictures were taken from some parts of the valley. It was caused primarily by the vegetation having significant coverage at the edge of the valley and the deeper areas. Hereinafter, we are planning to assign supplementary points with traditional geodetic survey as well.

The SfM model calculations was performed in Agisoft Photoscan software (Agisoft LLC 2016) using the selected most accurate parameterization (maximum key point limits, best quality, etc.). The reconstructed point cloud density was 1300 points/m^2 (Fig. 4) while the resolution of the derived digital surface model was 2.76 cm/pixel.

We classified few parts of the point cloud based on the colors in order to separate and

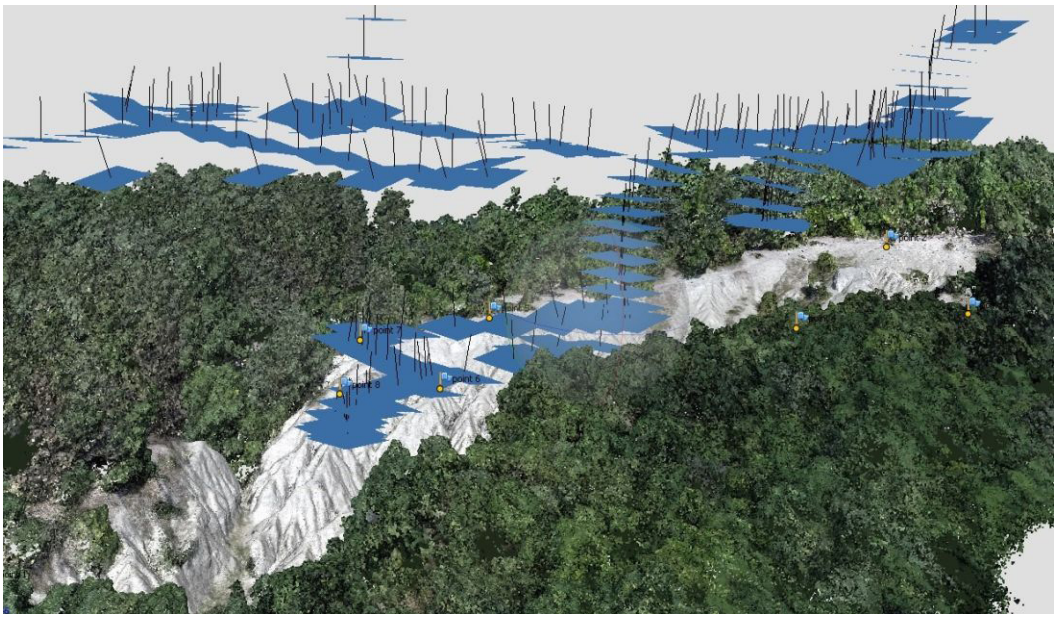

Fig. 3. Path of the multi-level flight above the sample area

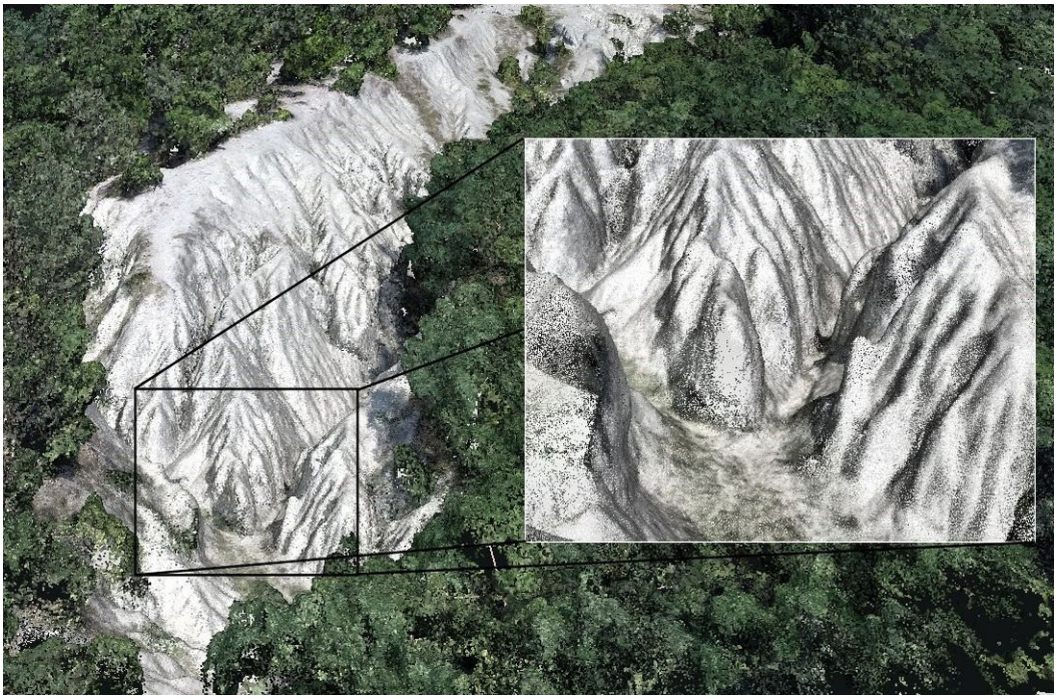

Fig. 4. Part of the dense point cloud

remove the points of vegetation from the white tuff surface and get a more accurate digital elevation model instead of the initial surface model. The parameterization of the dense point cloud generation was performed with the purpose of filtering out the single trees automatically.

Georeferencing of the model was based on 8 ground control points that are used for calculating exterior orientation parameters of the images (Miřijovský et al. 2015) so their accurate measurement was essential for the SfM modeling. However, referring to the common photogrammetric rules, for the exterior orientation GCPs should be distributed over the entire area (Miřijovský - Langhammer 2015) but the sample area had a relatively long and narrow shape (125 meters long but the width did not reach 30 meters in any parts) characterized by its morphological features (rill and gully erosion system); therefore, in this case the optimal placement of the GCPs was not reasonable. The surrounding forests also had a major contribution to this issue which was not suitable for placing GCP marks on the terrain. We used a Trimble S9 RTK GPS receiver for the reference survey that could guarantee a 2 cm precision.

We used circle-shaped and white control points with the diameter of 30 cm for the georeferencing. For the GCP design we had to consider the surface characteristics; thus, we supposed that GCPs with light colors would not have been recognizable on the light tuff surface due to the low contrast. Therefore, we prepared the GCPs with crosshair pattern with the combination of black and white colors that have a considerably high contrast (Fig. 5/a).

The light tuff material caused problems not only for designing the GCPs' pattern but also for the captured images as well. The surrounding forests induced stronger contrast against the badland surface; thus, it has a common occurrence that the aerial photographs become overexposed as a result of the interaction between the forest patches and the light tuff surface. These kind of pictures could not be used for the photogrammetric processing (Fig. 5/b.) so we had to compensate this phenomenon by the frequent changes in the direction and maneuvering over the valley during the multicopter flight.

For the geographic object-based image analysis of the ortophotograph we used

Fig. 5. Special GCP pattern designed for the bright surface (a); overexposed aerial image of the tuff surface (b)

eCognition Developer software (Nussbaum – Menz 2008) and the bottom-up region-merging technique of multiresolution segmentation for preparing the image segments.

We took into consideration the color and shape features as primary object forming features with the purpose of determining the spatial heterogeneity. At the processing phase we did not change the weighting factor values (blue: 1, green: 1, red: 1) of the true color ortophotograph. We performed the segmentation on five segmentation levels (scale parameter: 20, 50, 100, 200, 300) with defining the same homogeneity criteria for each scale parameters. The parameterization was implemented based on the literature (Burnett – Blaschke 2003; Platt – Schoennagel 2009) and empirically. During the segmentation we defined all the color and shape features with same weighting factor (0,5; 0,5) in all segmentation level; thus, both were suitable for separating the anthropogenic landscape elements with hard edges from the natural objects having "light" edges (Kressler – Steinnocher 2008).

The classified map was composed by involving the threshold values assigned to the image features (brightness, saturation). We defined three land cover categories: bare tuff surface, vegetation and not classified ('No data') pixels. The merging of the adjacent segments having the same land cover category was performed in ArcGIS software after exporting the results to vector-based GIS datasets. The map of results was composed in that software too.

3. Results and Discussion

The final SfM model is built up by more than 22 million points from which we derived the digital surface model with a resolution of 2.76 cm/pixel and the true ortophotograph with a resolution of 1.38 cm/pixel (Table 1).

In spite of the relatively small number of GCPs the mean error of georeferencing was vertically less than 4 cm; thus, we can expect that the local active surface development could be detected by a subsequent survey. The longitudinal shape of the valley and the resulting GCP distribution did not cause collinearity.

Table 1. Specifications of the SfM model (V: Vertical ; Hz: Horizontal)

Dense point cloud (point count)	22076701
Geometric resolution of the DSM (cm/pixel)	2.76
Geometric resolution of true ortophotograph (cm/pixel)	1.38
Number of GCPs	8
Mean error of GCPs (cm)	3.4 (V), 9.3 (Hz)

We determined that the reference points having an increased contrast provide substantially improved identification; therefore, their use is reasonable in the case of these homogenous and light surfaces. It can be also stated that the photogrammetric modelling of areas having this extremely high contrast implies special demands (i.e. flight path, local regulation of fly height) already during the aerial imaging.

Throughout the multiresolution segmentation we created increasingly large objects by merging the adjacent and spectrally most similar segments (Table 2). With the purpose of optimizing the classification we had minimized locally the mean heterogeneity of the resulting segments. We created spatially continuous, separate and homogenous regions, and we found the lower segmentation levels (scale factor: 20-50) overdetailed for the image classification, accordingly, we used the segmented image (Fig. 6) that had been made at the highest segmentation level (scale factor: 300). The segments with missing data, the bare greyish-white tuff surface and the vegetation cover were well identifiable visually on that image.

The errors of the photogrammetric processing resulted a 644 m^2 cover of image objects coverage from the 15 586 m^2 total area. Those segments were concentrated mainly at the forest cover surrounds the bare surfaces. Total area of the vegetation-

Table 2. Number of image objects generated by the multiresolution segmentation

Segmentation level	*Scale factor*	*Number of image objects*
1	20	264996
2	50	47115
3	100	13165
4	200	4264
5	300	2411

free rhyolite-tuff surfaces, made by different size of fragments, was 2087 m^2 that was fragmented by patches of herbaceous plants on silicate rocky grasslands and shrub/tree groups (Fig. 7).

Spreading of vegetation reduces the area of bare tuff surface and isolates the mosaics of the rhyolite-tuff. The area of the largest erosion-field was 1893 m^2, curved and sickle-shaped with an E-SW orientation. Erosion forms of the rhyolite-tuff caused the slight horizontal and vertical fragmentation of the surface. Classification of the ortophotograph was difficult due to the rills, the occasionally several meters deep gullies and the shadow of tuff ridges and pyramids remained between valleys. The canopy and shadows of the woody plants form dark pixel-groups since their reflectance was similar in this visible spectral range; thus, on the segmented image (Fig. 6) the majority of image-objects that had been classified as linear, curved or bough-like vegetation, which is wedging to the uncovered bare tuff surface, were actually parts of the erosion-surface. 12 855 m^2 of the study area was vegetated by thermophilic oak forests, planted black locusts, black pines and rock-grassland mosaics.

Image objects that had been formed by several scale-factor and having different spectral and shape homogeneity could be applicable for identifying the micro- and macroforms of erosion surfaces, the bare and covered (pioneer herbaceous vegetation) patches, individual and groups of trees, and the shadow of canopy. Primarily, shadow effect on the high resolution remote sensing data made the classification more difficult and reduced its accuracy in the case of surfaces that were covered by woody vegetation,

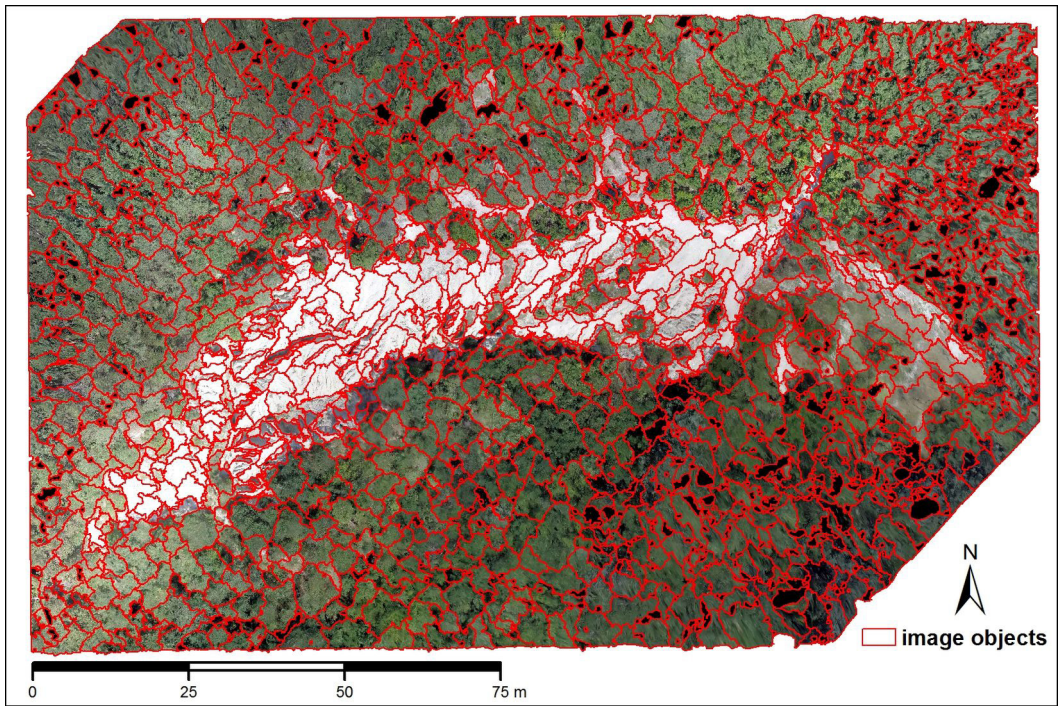

Fig. 6. Segmented image used for the classification

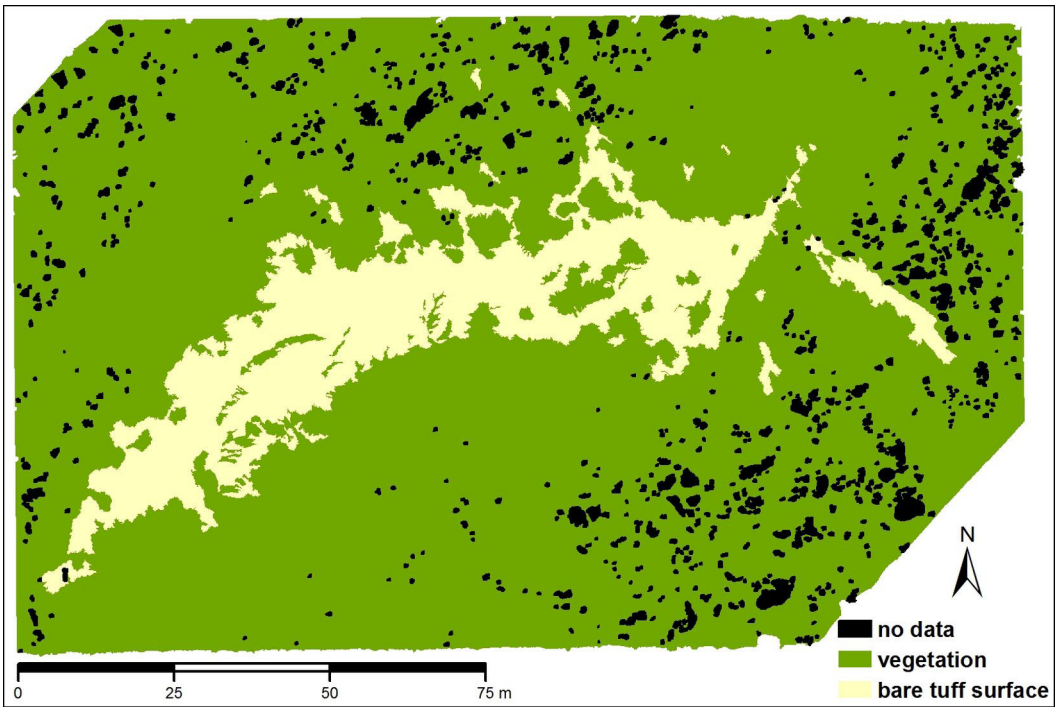

Fig. 7. Land cover map of the study area based on the classification

horizontally and vertically fragmented and which were characterized by erosion and/or accumulation landforms. The shape and size of shadows were influenced by mainly the date of flight, the landform elements and the orientation of emerging objects.

The identification of vegetated and bare surfaces could be improved by increasing the spectral resolution of the ortophotograph and involving spectral indices. The digital surface and terrain models and the derived and normalized elevation model supports the classification of higher and lower reliefs, the positive and negative landform elements and the vertical fragmentation of vegetation (levels of grassland, shrub, canopy).

4. Conclusions

This study provided a detailed overview about the initial UAS survey of the Kazár badland. It turned out that the outstanding light tuff surface with the surrounding forests could cause overexposed imagery but manual flight control serves as a solution for performing a survey that is adjusted to the relief characteristics of the landform. Black and white or similar pair of colors with high contrast is recommended for the effective GCP identification. The geographic object-based image analysis method allowed us to classify the ortophotograph well and separate the tuff surface and the vegetation. The final digital elevation model in combination with the subsequent UAS surveys will be used for detecting the recent erosional processes of the Kazár badland in the future.

Acknowledgement

This work was supported by the University of Debrecen (RH/751/2015).

5. References

Aber, J.S. – Marzolff, I. – Ries, J.B. (2010): Small Format Aerial Photography: Principles, techniques and geoscience applications. Elsevier, 256 p.

Agisoft LLC (2016): Agisoft Photoscan User Manual. Standard Edition, Version 1.2.: http://www.agisoft.com/pdf/photoscan_1_2_en.pdf

Blaschke, T. – Strobl, J. (2001): What's wrong with pixels? Some recent developments interfacing remote sensing and GIS. GIS – Zeitschrift für Geoinformationssysteme. 6(1): 12-17.

Burnett, C. – Blaschke, T. (2003): A multi-scale segmentation/object relationship modelling methodology for landscape analysis. Ecological Modelling. 168(3): 233-249.

Caraballo-Arias, N.A. – Conoscenti, C. – Di Stefano, C. – Ferro, V. (2015): A new empirical model for estimating calanchi Erosion in Sicily, Italy. Geomorphology. 231: 292-300.

Colomina, I. – Molina, P. (2014): Unmanned aerial systems for photogrammetry and remote sensing: A review. ISPRS Journal of Photogrammetry and Remote Sensing. 92: 79-97.

Conoscenti, C. – Di Maggio, C. – Rotigliano, E. (2008): Soil erosion susceptibility assessment and validation using a geostatistical multivariate approach: a test in Southern Sicily. Natural Hazards. 46: 287-305.

Conoscenti, C. – Angileri, S. – Cappadonia, C. – Rotigliano, E. – Agnesi, V. – Märker, M. (2014): Gully erosion susceptibility assessment by means of GIS-based logistic regression: A case of Sicily (Italy). Geomorphology. 204: 399-411.

Czigány, Sz. – Pirkhoffer, E. – Nagyváradi, L. – Hegedűs, P. – Geresdi I. (2011): Rapid screening of flash flood-affected watersheds in Hungary. Zeitschrift für Geomorphologie. 55(Suppl.1): 1-13.

Czimber, K. (2009): Új, általános célú képosztályozó kifejlesztése nagyfelbontású, textúrával rendelkező digitális képek feldolgozására (Development of a new, general image classifier to process high-resolution, textured digital images). Geomatikai Közlemények. 12: 249-258. (in Hungarian)

d'Oleire-Oltmanns, S. – Marzolff, I. – Peter, K.D. – Ries, J.B. (2012). Unmanned Aerial Vehicle (UAV) for Monitoring Soil Erosion in Morocco. Remote Sensing. 4: 3390-3416.

Dragut, L. – Eisank, C. (2012): Automated object-based classification of topography from SRTM data. Geomorphology. 141-142: 21-33.

Farabegoli, E. – Agostini, C. (2000): Identification of calanco, a badland landform in the Northern Apennines, Italy. Earth Surface Processes and Landforms. 25: 307-318.

Gómez-Gutierrez, Á. – de Sanjosé-Blasco, J.J. – de Matías-Bejarano, J. – Berenguer-Sempere, F. (2014): Comparing Two Photo-Reconstruction Methods to Produce High Density Point Clouds and DEMs in the Corral del Veleta Rock Glacier (Sierra Nevada, Spain). Remote Sensing. 6: 5407-5427.

Horváth, G. – Karancsi, Z. (2011): Intensity of the anthropogenic effects on a small landscape unit in North Hungary. Zeitschrift für Geomorphologie. 55 (Suppl.1): 37-50.

Karancsi, Z (2010): Agriculture: deforestation. In: Szabó, J. – Dávid, L. – Lóczy, D. (Eds)(2010): Anthropogenic geomorphology: a guide to manmade landforms. Springer, Dordrecht. 95-112.

Karátson, D. (2006): Aspects of Quaternary relief evolution of Miocene volcanic areas in Hungary: A review. Acta Geologica Hungarica. 49(4): 285-309.

Kressler, F. – Steinnocher, K. (2008): Object-oriented analysis of image and LiDAR data and its potential for a dasymetric mapping application. In: Blaschke, T., Lang, S., Hay, G.J. (Eds.)(2008): Object-Based Image Analysis: Spatial Concepts for Knowledge-Driven Remote Sensing Applications. Springer-Verlag, Berlin-Heidelberg. 611-624.

Lopez Saez, J. – Corona, C. – Stoffel, M. – Rovéra, G. – Astrade, L. – Berger, F. (2011): Mapping of erosion rates in marly badlands based on a coupling of anatomical changes in exposed roots with slope maps derived from LiDAR data. Earth Surface Processes and Landforms. 36: 1162-1171.

Mészáros, J. – Árvai, M. – Kohán, B. – Deák, M. – Nagy, B. (2016): UAV based 3D digital surface model to estimate paleolandscape in high mountainous environment. Geophysical Research Abstracts 18: Paper 15430. EGU General Assembly 2016. Wien, Austria.

Miřijovský, J. – Šulc Michalková, M. – Petyniak, O. – Máčka, Z. – Trizna, M. (2015): Spatiotemporal evolution of a unique preserved meandering system in Central Europe - The Morava River near Litovel. Catena. 127: 300-311.

Miřijovský, J. – Langhammer, J. (2015): Multitemporal Monitoring of the Morphodynamics of Mid-Mountain Stream Using UAS Photogrammetry. Remote Sensing. 7: 8586-8609.

Nadal-Romero, E. – Regüés, D. – Martí-Bono, C. – Serrano-Muela, P. (2007): Badland dynamics in the Central Pyrenees: temporal and spatial patterns of weathering processes. Earth Surface Processes and Landforms. 32: 888-904

Nadal-Romero, E. – Petrlic, K. – Verachert, E. – Bochet, E. – Poesen, J. (2014): Effects of slope angle and aspect on plant cover and species richness in a humid Mediterranean badland. Earth Surface Processes and Landforms. 39: 1705-1716.

Nadal-Romero, E. – Revuelto, J. – Errea, P. – López-Moreno, J.I. (2015): The application of terrestrial laser scanner and SfM photogrammetry in measuring erosion and deposition processes in two opposite slopes in a humid badlands area (central Spanish Pyrenees). SOIL. 1: 561-573.

Neugirg, F. – Stark, M. – Kaiser, A. – Vlacilova, M. – Della Seta, M. – Vergari, F. – Schmidt, J. – Becht, M. – Haas, F. (2016): Erosion processes in calanchi in the Upper Orcia Valley, Southern Tuscany, Italy based on multitemporal high-resolution terrestrial LiDAR and UAV surveys. Geomorphology. 269: 8-22.

Nussbaum, S. – Menz, G. (2008): eCognition Image Analysis Software. In: (Nussbaum, S. – Menz, G. (Eds.)(2008): Object-Based Image Analysis and Treaty Verification. Part I. Springer. 29-39.

Openshaw, S. (1984): The Modifiable Areal Unit Problem. Concepts and Techniques in Modern Geography (CATMOG) 38. Geo Books, Norwich, 41 p.

Pintér, Z. – Prakfalvi, P. – Karancsi, Z. – Horváth, G. (2009): Medves-vidéki riolittufák eróziós formakincse (Erosional forms of rhyolite tuffs in the Medves region). Földrajzi Közlemények. 133(3): 219-238 (in Hungarian)

Pintér, Z. – Horváth, G. – Jakab, G. – Karancsi, Z. (2015): Rhyolite Badland at Kazár. In: Lóczy, D. (ed) Landscapes and Landforms of Hungary, World Geomorphological Landscapes. Springer International Publishing Switzerland. 149-155.

Platt, R.V. - Schoennagel, T. (2009): An object-oriented approach to assessing changes in tree cover in the Colorado Front Range 1938–1999. Forest Ecology and Management. 258(7): 1342-1349.

Regüés, D, Pardini, G, Gallart, F. (1995): Regolith behaviour and physical weathering of clayey mudrock as dependent on seasonal weather conditions in a badland area at Vallcebre, Eastern Pyrenees. Catena. 25(1-4): 199-212.

Stöcker, C. – Eltner, A. – Karrasch, P. (2015): Measuring gullies by synergetic application of UAV and close range photogrammetry - A case study from Andalusia, Spain. Catena. 132: 1-11.

Telbisz, T. – Mari, L. – Székely, B. (2012): Torockói-hegység völgyhálózat fejlődése (Valley network evolution of the Trascău Mountains). Földrajzi Közlemények (Geographical Review). 136(1): 22-36. (in Hungarian)

Török, Á. – Vogt, T. – Löbens, S. – Forgó, L.Z. – Siegesmund, S. – Weiss, T. (2005): Weathering forms of rhyolite tuff and changes in physical properties. Zeitschrift der Deutschen Geologischen Gesellschaft. 156(1): 177-187.

Westoby, M.J. – Brasington, J. – Glasser, N.F. – Hambrey, M.J. – Reynolds, J.M. (2012): 'Structure-from-Motion' photogrammetry: A low-cost, effective tool for geoscience applications. Geomorphology. 179: 300-314.